O. Svoboda[1,2,*], J. Adam[1,3], M. Bielewicz[4], S. Kilim[4],
A. Krása[1], M. I. Krivopustov [3], M. Majerle[1], V. I. Stegailov[3],
E. Strugalska-Gola[4], A. A. Solnyshkin [3], M. Szuta[4],
V. M. Tsoupko-Sitnikov[3], V. Wagner[1,2]

THE STUDY OF SPALLATION REACTIONS, NEUTRON PRODUCTION AND TRANSPORT IN A THICK LEAD TARGET AND URANIUM BLANKET DURING 1.6 AND 2.52 GeV DEUTERON IRRADIATION

On behalf of the Collaboration «Energy and Transmutation
of Radioactive Waste»

[1]Nuclear Physics Institute of the Academy of Sciences of the Czech
Republic, Řež, Czech Republic
[2]Faculty of Nuclear Sciences and Physical Engineering, Czech Technical
University in Prague, Czech Republic
[3]Joint Institute for Nuclear Research, Dubna
[4]Institute of Atomic Energy, Otwock-Świerk, Poland
*E-mail: svoboda@ujf.cas.cz

Свобода О. и др. (по поручению коллаборации «Энергия   E15-2011-39
и трансмутация радиоактивных отходов»)

Изучение спалогенных реакций, образование нейтронов и
их прохождение в толстой свинцовой мишени и урановом бланкете
в процессе облучения дейтронами при энергии 1,6 и 2,52 ГэВ

Для изучения нейтронных полей в установке «Энергия плюс трансмутация», состоящей из толстой свинцовой мишени и бланкета из натурального урана, использовались нейтронно-активационные детекторы. Установка облучалась пучками дейтронов при энергии 1,6 и 2,52 ГэВ на ускорителе нуклотрон. Эксперимент является частью систематического изучения нейтронных полей и трансмутации с использованием протонных и дейтронных пучков в диапазоне энергий от 0,7 до 4 ГэВ. Экспериментальные данные сравнивались с результатами расчетов МСNPX и данными предыдущих экспериментов. Наблюдалось хорошее согласие в пределах статистических неопределенностей.

Работа выполнена в Лаборатории ядерных проблем им. В. П. Джелепова ОИЯИ.

Svoboda O. et al. (On behalf of the Collaboration   E15-2011-39
«Energy and Transmutation of Radioactive Waste»)

The Study of Spallation Reactions, Neutron Production
and Transport in a Thick Lead Target and Uranium Blanket
during 1.6 and 2.52 GeV Deuteron Irradiation

Neutron activation detectors were used to study the neutron field in the setup «Energy plus Transmutation» consisting of a thick lead target and natural uranium blanket. This setup was exposed to 1.6 and 2.52 GeV deuteron beam from the Nuclotron accelerator. The experiment is a part of systematic study of neutron field and transmutation using proton and deuteron beams in the energy range from 0.7 up to 4 GeV. The experimental data were compared with the results of the MCNPX simulations and with the data from the previous experiments. A good agreement within the statistical uncertainties was observed.

The investigation has been performed at the Dzhelepov Laboratory of Nuclear Problems, JINR.

INTRODUCTION

Spallation reaction as a perspective source of neutrons has been studied with an increased interest in the last decade. These studies are motivated by the need of high neutron fluxes for material research, transmutation of nuclear waste or production of nuclear fuel from thorium. New spallation sources are planned (European Spallation Source) or already commissioned (American Spallation Neutron Source) to fulfill scientific requirements. With advances in accelerator technology, Accelerator Driven Systems (ADS), due to their high safety and unique properties, seem to be a perspective energy source for the future.

This publication is a part of the international research program «Energy and Transmutation of Radioactive Waste». Within this project, groups from 15 countries study various aspects of spallation reaction, neutron production, transport and its usage for transmutation of nuclear waste. Six different setups of massive target surrounded with blanket and neutron moderator are used to measure differential as well as global data for ADS.

The setup called «Energy plus Transmutation» («E + T») is a system of thick lead target surrounded by a subcritical uranium blanket. It was already irradiated with protons (0.7–2 GeV), results are described, e.g., in [1–4], or [5]. Experiments with deuterons were the next logical step in the systematic studies of spallation reaction. The «E + T» setup in the previous years was irradiated by 1.6–4 GeV deuterons and some of the results of the 1.6 GeV and 2.52 GeV irradiations have been described in this paper. All experiments were carried out at the Joint Institute for Nuclear Research (JINR), Dubna, Russia.

Within broad scientific program of the E & T RAW group, we aimed to study high energy neutron field in this complex setup. The obtained data were used for testing predictions of computer code MCNPX [6] (the «E + T» setup was acknowledged as an IAEA benchmark target). Experimental results combined with simulation were used for experimental neutron multiplicity determination and for tests of high energy neutron cross sections of selected reactions.

EXPERIMENTAL SETUP

The «E + T» setup consists of a cylindrical lead target (84 mm diameter, 480 mm total length) and a surrounding subcritical uranium blanket (206.4 kg of natural uranium). The target and blanket are divided into four sections. Between the sections there are 8 mm gaps for user's samples, detectors and emulsions. Each section contains target cylinder of 114 mm long and 30 identical natural uranium rods, which are encased in a hexagonal steel container with a wall thickness of 4 mm. The front and back of each section are covered with hexagonal aluminum plate of 6 mm thick. The four target-blanket sections are mounted along the target axis on a wooden plate of 68 mm thickness, which is moreover covered with 4 mm thick steel sheet. Uranium rods are hermetically encapsulated in aluminum cladding of 1 mm thickness, respectively, 1.2 mm at the bases. Each rod has an outer diameter of 36 mm, a length of 104 mm, and a weight of 1.72 kg. Density of the uranium is considered to be 19.05 $g \cdot cm^{-3}$.

Around the blanket there is a radiation shielding consisting of a wooden box, cadmium plates and polyethylene $((CH_2)_n)$ in the box walls. Cadmium plates have a thickness of 1 mm and are mounted on the inner walls of the box. Polyethylene has a density of 0.8 $g \cdot cm^{-3}$ and is granulated. On the floor inside the shielding box a 38 mm thick textolite plate is placed. The shielding moderates and absorbs only a part of the high energy neutrons emerging from the setup, because there is a dosimetry limit on the beam flux.
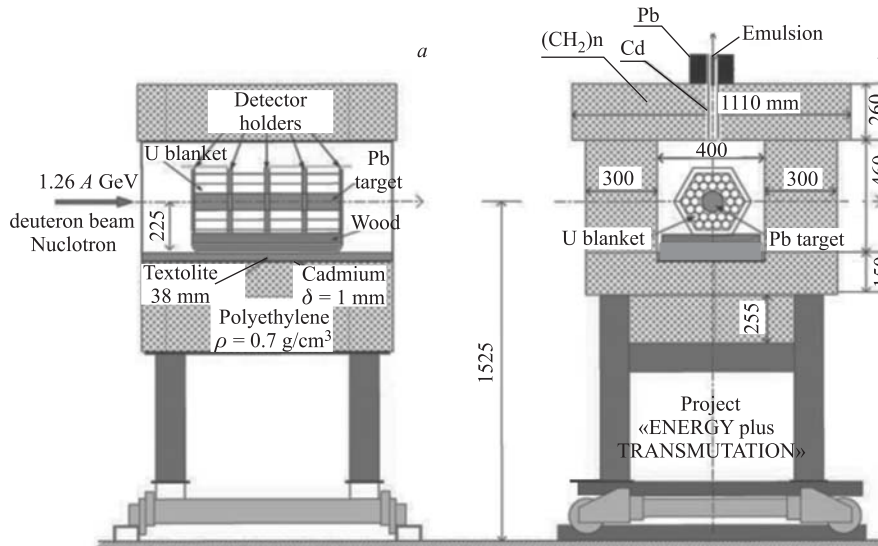
Fig. 1. Cross sectional side view (left) and front view (right) at the «Energy plus Transmutation» setup. All dimensions are in millimeters

2

The whole assembly is mounted on an iron stand and can be moved on rails within the experimental hall F3. Schematic drawing of the «E + T» setup can be seen in Fig. 1.

The detailed analysis of the influence of different setup parts and uncertainties in their geometrical and physical definitions on the neutron flux was done in the MCNPX simulation code [7].

HIGH ENERGY NEUTRON DETECTORS

The neutron activation method was used to measure high energy neutron production and transport. Activation detectors in the form of foils were placed in the gaps between the «E + T» setup sections. Example of foil placement can be seen in Fig. 2, list of all used samples is shown in Tables 2 and 3.

Activation samples were made of aluminum, gold, bismuth, indium, tantalum and yttrium. These elements were chosen, because they are mostly naturally mono-isotopic or one of the isotopes is dominant. They are also cheap, relatively nontoxic and have good physical properties (melting point, rollable). Further dominant criteria for choosing these elements were the decay times of the isotopes, that were produced due to (n, xn) reactions. Activation samples had a square shape of 20 mm size (Au, Al and Ta samples), 25 mm size (Bi samples), and 12.5 mm size (In samples). Yttrium was in form of small compressed pills. Chemical purity of the materials was better than 99.99%.

Average weight of used foils was 0.3 g for Au, 0.6 g for Al, 6.5 g for Bi, 0.6 g for In, 0.8 g for Ta and 1.1 g for Y foils. The foils for the irradiation were wrapped twice in the paper. The inner paper minimalized the transport of the fission products and produced isotopes out of the foil and also between different foils; moreover, the HPGe detector contamination was excluded. The outer paper (removed after the irradiation) minimalized contamination of the samples by radioisotopes coming from the setup.

Complicated neutron field was produced inside the setup during irradiation. This field induced in our activation sensors a lot of various nuclear reactions, mainly of (n, γ), (n, α), (n, p) and (n, xn) type. Thus, many new radioactive nuclei were produced in each sample. We learned about their abundance in the sample from the characteristic γ-ray spectrum they have emitted during the decay (irradiated foils were measured on HPGe detectors).

Used HPGe detectors were of the Ortec GMX type with the small Dewar flask, for more parameters see Table 1. One of the detectors was placed in a lead shielding with the back wall opened. This shielding partially suppressed the background; moreover it shielded the personnel from measured samples. The detector systems were calibrated using well-defined [54]Mn, [57]Co, ^{60}Co, [88]Y, [109]Cd, [113]Sn, [133]Ba, ^{137}Cs, [139]Ce, [152]Eu, [228]Th, and [241]Am sources which have γ lines
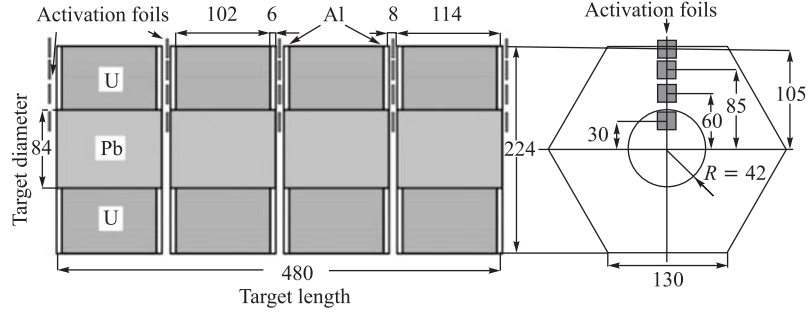
Fig. 2. The placement of the aluminum, gold and tantalum activation foils. The others were placed in the same way, but in another direction (e.g., bismuth and indium in the right-down direction from the target axis)

Table 1. Parameters of used HPGe detectors

Manufacturer/Name	ORTEC (new1)	ORTEC (new2)
Type	GMX-20190	GMX-30
Resolution, keV ($E_\gamma = 1332$ keV)	1.80	1.80
Relative efficiency [%] ($E_\gamma = 1332$ keV)	28.3	32.9
Coating, mm	0.50 — Be	1.27 — Al
Dead Ge layer, μm	0.3	0.3
Detector bias supply	ORTEC 659	ORTEC 660
Spectroscopy preamplifier	Canberra 2024	Canberra 2026
ADC	Multichannel buffer — ORTEC 919	
Bias voltage, V	-4800	-4000
Shaping time, μs	4	3

ranging from 80 up to 2700 keV. The obtained calibration γ spectra were analyzed and the net peak areas were calculated using the program DEIMOS32 [8]. All necessary corrections on possible coincidences and background contributions were made. The accuracy of the efficiency determination is $\sim 2\%$ for further geometries and $\sim 3\%$ for the nearest geometry. After all measurements the calibration was checked once more to control the calibration stability. Calibration curves were put into the Excel as an Add-in.

Normally written foils were placed in the upwards direction like in Fig. 2. Bold-written foils were placed in the right-down direction under the angle of $30°$ from horizontal. Italic-written foils were placed in the left-up direction under the angle of $30°$ from vertical direction.

4

Table 2. Foils placement in the «E + T» setup during 1.6 GeV deuteron experiment

	Distance from the target axis, cm	Foil labels in 1.6 GeV deuteron experiment					
1st plane	0						*Y_5*
	3	Al1	Au1	Ta01	**Bi1**	**In1**	*Y_8*
	6	Al2	Au2	Ta02			*Y_13*
	8.5	Al3	Au3	Ta03			*Y_15*
	10.5						*Y_22*
	10.7	Al4	Au4	Ta04			
	13.5						*Y_9*
	up						*Y_19*
	down						*Y_21*
	left						*Y_38*
	right						*Y_20*
2nd plane	0						*Y_10*
	3	Al5	Au5	Ta05	**Bi2**	**In2**	*Y_1*
	6	Al6	Au6	Ta06	**Bi3**	**In3**	*Y_6*
	8.5	Al7	Au7	Ta07	**Bi4**	**In4**	*Y_7*
	10.5						*Y_32*
	10.7	Al8	Au8	Ta08			
	11.5				**Bi5**	**In5**	
	13.5						*Y_2*
3rd plane	0						*Y_4*
	3	Al9	Au9	Ta09	**Bi6**	**In6**	*Y_35*
	6	Al10	Au10	Ta10			*Y_36*
	8.5	Al11	Au11	Ta11			*Y_18*
	10.5						*Y_33*
	10.7	Al12	Au12	Ta12			
	13.5						*Y_27*
4th plane	0						*Y_41*
	3	Al13	Au13	Ta13	**Bi7**	**In7**	*Y_25*
	6	Al14	Au14	Ta14			*Y_34*
	8.5	Al15	Au15	Ta15			*Y_37*
	10.5						*Y_40*
	10.7	Al16	Au16	Ta16			
	13.5						*Y_16*
5th plane	0						*Y_17*
	3	Al17	Au17	Ta17	**Bi8**	**In8**	*Y_11*
	6	Al18	Au18	Ta18			*Y_29*
	8.5	Al19	Au19	Ta19			*Y_3*
	10.5						*Y_39*
	10.7	Al20	Au20	Ta20			
	13.5						*Y_12*

Table 3. Foils placement in the «E + T» setup during 2.52 GeV deuteron experiment

	Distance from the target axis, cm	Foil labels in 2.52 GeV deuteron experiment					
1st plane	0						Y_32
	3	Al31	Au1	Ta01	**Bi1**	**In1**	Y_34
	6	Al32	Au2	Ta02			Y_15
	8.5	Al33	Au3	Ta03			Y_16
	10.5						Y_6
	10.7	Al34	Au4	Ta04			
	13.5						Y_7
2nd plane	0						Y_9
	3	Al35	Au5	Ta05	**Bi2**	**In2**	Y_12
	6	Al36	Au6	Ta06	**Bi3**	**In3**	Y_31
	8.5	Al37	Au7	Ta07	**Bi4**	**In4**	Y_14
	10.5						Y_19
	10.7	Al38	Au8	Ta08			
	11.5				**Bi5**	**In5**	
	13.5						Y_33
3rd plane	0						Y_23
	3	Al39	Au9	Ta09	**Bi6**	**In6**	Y_35
	6	Al40	Au10	Ta10			Y_24
	8.5	Al11	Au11	Ta11			Y_29
	10.5						Y_1
	10.7	Al12	Au12	Ta12			
	13.5						Y_3
4th plane	0						Y_25
	3	Al13	Au13	Ta13	**Bi7**		Y_36
	6	Al14	Au14	Ta14			Y_22
	8.5	Al15	Au15	Ta15			Y_8
	10.5						Y_18
	10.7	Al16	Au16	Ta16			
	13.5						Y_5
5th plane	0						Y_17
	3	Al17	Au17	Ta17	**Bi8**		Y_26
	6	Al18	Au18	Ta18			Y_20
	8.5	Al19	Au19	Ta19			Y_11
	10.5						Y_21
	10.7	Al20	Au20	Ta20			
	13.5						Y_13
1 m in front of the target	centre						Y_2
	3 cm up						Y_10
	3 cm down						Y_28
	3 cm left						Y_27
	3 cm right						Y_4

6

EVALUATION OF DETECTORS

After the irradiation, activated detectors were transported to the spectroscopic laboratory at JASNAPP in order to measure their γ activities with HPGe detectors. Almost all samples were measured twice. First measurement followed shortly after the irradiation and lasted only a few minutes, the second one was performed days up to weeks after irradiation. That way we could detect maximum of produced isotopes. Unfortunately, there was a two hours gap between the exact end of the irradiation and the start of the measurement, in which we had to wait for the radioactivity decrease of the setup (before this we were not allowed to manipulate with the setup and our samples). This is the reason for unobserving of the isotopes with half-life shorter than approximately one hour.

To analyze γ-ray spectra and to determine net peak areas, the computer program DEIMOS32 was used. Corrections for decay, gamma-line intensity, possible coincidence effects (coincidence summing and background contribution), detector efficiency, beam instability, nonpoint-like emitters, self-absorption and dead time correction were applied to obtain the total number of nuclei of certain isotope — the so-called yield. This yield was then normalized to 1 g of activation foil and to 1 primary beam deuteron (the measured beam intensity was used). After this, we could compare results among other «Energy plus Transmutation» experiments. The final formula for yield calculation is shown below:

$$N_{\text{yield}} = \frac{S_p C_{\text{abs}}(E) B_a}{I_\gamma \varepsilon_P(E) \text{Coi} C_{\text{area}}} \frac{t_{\text{real}}}{t_{\text{live}}} \frac{1}{m_{\text{foil}}} \frac{1}{I_d} \frac{e^{(\lambda \cdot t_0)}}{1 - e^{(-\lambda \cdot t_{\text{real}})}} \frac{\lambda t_{\text{irr}}}{1 - e^{(-\lambda \cdot t_{\text{irr}})}}, \quad (1)$$

where S_p — peak area; C_{abs} — self-absorption correction; B_a — beam correction; I_γ — gamma-line intensity; C_{area} — nonpoint-like emitter correction;
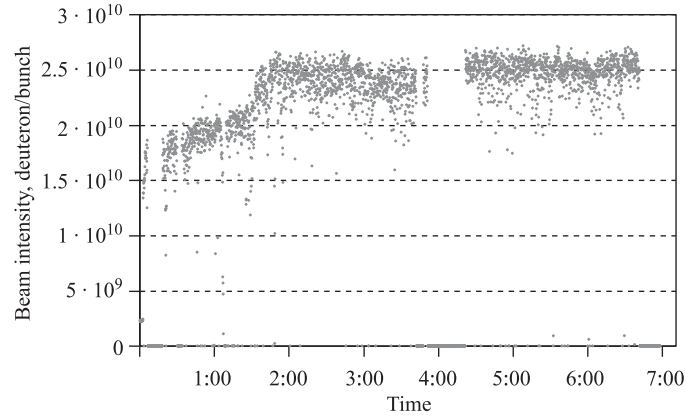
Fig. 3. Beam intensity during 1.6 GeV deuteron irradiation of the «E + T» setup

7
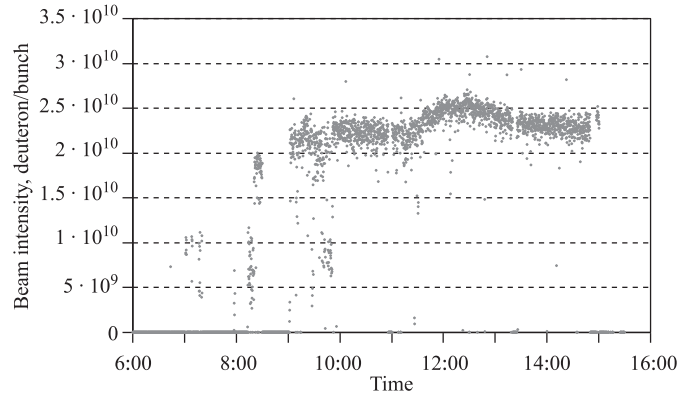
Fig. 4. Beam intensity during 2.52 GeV deuteron irradiation of the «E + T» setup

Coi — correction for coincidences; λ — decay constant; t_{irr} — irradiation time; t_{real} — real measurement time; t_0 — cooling time; t_{live} — live time of the detector; m_{foil} — weight of the foil; I_d —- number of neutrons in the beam.

Beam correction and square emitter correction are described in [4] (Figs. 3 and 4).

IRRADIATION AT NUCLOTRON

Irradiation of the «E + T» setup was carried out at the Veksler and Baldin Laboratory of High Energy Physics by 1.6 and 2.52 GeV deuteron beam extracted from the Nuclotron accelerator (Table 4). These deuteron irradiations were a continuation of the previous proton experiments, in which the «Energy plus Transmutation» setup was irradiated by 0.7; 1; 1.5; and 2 GeV protons.

Table 4. Irradiation parameters of deuteron experiments at the «E + T» setup

Deuteron beam energy, GeV	1.6	2.52
Beam start	17.12.2006 23:55:33	30.11.2005 7:01:11
Beam end	18.12.2006 6:42:18	30.11.2005 15:00:48
Time of irradiation, h	6.7	8
Beam intensity measured by operators, 10^{13}	5.8	4.7

8

BEAM MONITORS

Knowledge of the beam intensity, position and shape is crucial for the experiment evaluation. Significant influence of the beam position on experimental results was observed in the activation detectors placed close to the target axis, MCNPX simulations were done to assess this effect.

Beam Position. The geometrical adjustment of the experimental setup with respect to the deuteron beam was tuned before the irradiation by means of sensitive Polaroid films. The films were placed directly in front of the target to see the position and profile at the point, where the beam entered the target. Another Polaroid film was placed behind the target to check the direction of the beam in the target. Beam parameters during the irradiation were determined independently from solid-state nuclear track detectors (Belarus group — I. Zhuk) and from a set of copper activation foils.

The copper foils were placed directly in front of the target and behind it. The copper was chosen, because in interaction with deuterons a lot of radioactive isotopes are produced, but none of them are produced by neutrons in significant ammount. On the other hand, no experimental cross sections are known for interaction of relativistic deuterons and copper. We could make only relative comparison between the foils.

For measurement of the beam position in front of the target, 60×60 mm^2 copper foil was used. Thickness of the foil was 100 μm. The foil was cut after the irradiation into 20×20 mm^2 pieces (totally 9 pieces), and each piece was measured separately. Following isotopes were observed: ^{43}K, ^{47}Sc, ^{48}Sc, ^{44m}Sc, ^{44}Sc, ^{48}V, ^{48}Cr, ^{52}Mn,^{58}Co, ^{56}Co, ^{55}Co, ^{57}Ni, and ^{61}Cu. Totally 19 lines were used for the final evaluation. The above-mentioned isotopes were observed only
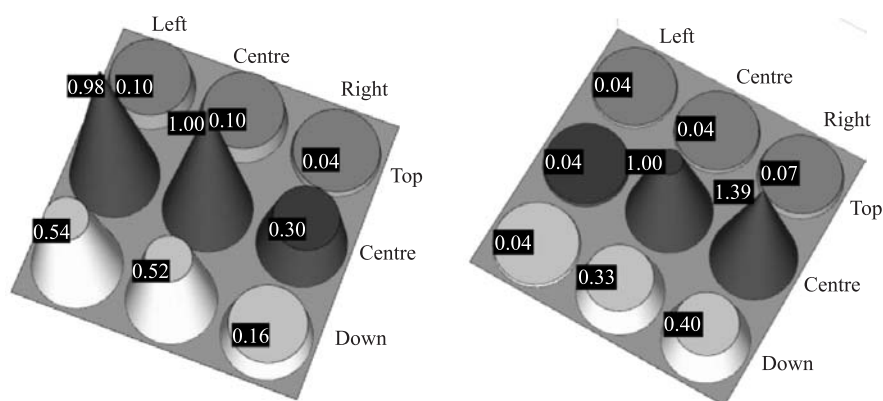
Fig. 5. Weighted average over relative yields in the forward Cu beam monitor during 1.6 GeV (left) and 2.52 GeV (right) experiments

9

in the most active foils, in other foils they were not detected or were on the level of detection limit (this represents relative production between 1 and 6 % in non-hit foils). None of these isotopes was visible in all foils and with similar activities; this led us to the presumption that all the isotopes we used were produced by the deuterons from the beam and not by back-scattered neutrons from the target. Yields of each isotope were normalized to the most active foil and a weighted average over all reactions and used gamma lines was made. To calculate the beam profile area and its displacement we used two assumptions (simplifications) — the beam profile is of a circular shape and the deuteron distribution inside the profile has 3D Gauss shape (Fig. 5).

Beam Intensity. Beam intensity was measured using aluminum foils. We used a square foil $100 \times 100 \times 0.2$ mm^3 placed a few meters in front of the setup. W. Westmeier used concentric aluminum rings placed close to ours. Number of neutrons coming from the target is negligible at this distance.

Cross section of the $^{27}\text{Al}(d, 3p2n)^{24}\text{Na}$ reaction is the only known cross section in the region of GeV energies of deuterons with suitable half-life and energies of gammas. It was measured by J. Banaigs [9] at deuteron energy 2330 MeV (15.25 ± 1.5 mbarn).

For the gamma measurement on the detector we middled the foil few times to get a dimension approximately $25 \times 25 \times 3$ mm^3. We measured this packed foil on the detector several times in various geometries (and also on different detectors during the 2.52 GeV experiment) to suppress the uncertainty coming from detector calibration. Beam intensity N_d was calculated according to the following equation (2), where N_{yield} (of ^{24}Na) is calculated using Eq. (1):

$$N_d = \frac{N_{\text{yield}} S A}{\sigma N_A}, \tag{2}$$

where S — area of the foil; A — molar weight; N_A — Avogadro number; σ — $^{27}\text{Al}(d, 3p2n)^{24}\text{Na}$ reaction cross section.

We tried to calculate the beam intensity using also other reactions in the Al monitor and in the copper monitor used for the beam shape and profile determination. There are no experimental data for cross section of deuterons and copper (or aluminum, except those leading to ^{24}Na), but a lot of data exist for protons on copper and aluminum. It is possible to recalculate the cross sections from proton to deuteron using the method proposed by J. Blocki [10].

The cross-section recalculation is based on the presumption that there is a fixed ratio between the inelastic cross section for proton and deuteron (at relativistic energies two nucleons in ^2H behave as two separate items). The cross section for protons and deuterons seems to change slowly and their curves run parallel at GeV energies. We have started from already mentioned reaction $^{27}\text{Al}(d, 3p2n)^{24}\text{Na}$, where we know the cross section for deuterons at 2330 MeV (Banaigs, [9]). We found cross section for protons leading also to ^{24}Na (reaction

10

^{27}Al($p, 3pn$)^{24}Na) at similar energy 1200 MeV: Dittrich B. [11] — 12 mbarn, Michel R. [12] — 10.8 mbarn, and Titarenko Yu. [13] — 12.9 mbarn. Mean cross-section value is 11.9 mbarn. The ratio between the deuteron and proton cross sections is thus 1.282 (this should be the same for all reactions on Al). With this ratio we multiplied cross sections of proton induced reactions ^{27}Al($p, 3p3n$)^{22}Na and ^{27}Al($p, 10p10n$)^{7}Be and calculated beam intensity from the ^{22}Na and ^{7}Be yields produced by deuteron beams. Differences from the directly evaluated intensity were smaller than 4% at the ^{22}Na and 2% at ^{7}Be in the case of the 1.6 GeV deuteron experiment. During the 2.52 GeV deuteron experiment no long-time measurements of Al beam monitors were done (because of the lack of time), so it was not possible to test this procedure.

Finally, we tried to calculate deuteron beam intensity from the copper foils. No experimental cross sections for suitable ^{nat}Cu(d, x) reactions are known at the used energy region, so we had to calculate our own cross sections. The above-mentioned procedure was not usable because of missing cross sections, so we assumed the beam intensity in the 2.52 GeV deuteron experiment was determined properly. With this beam intensity we have calculated cross sections of various reactions observed on copper during the 2.52 GeV deuteron experiment. These cross sections were shifted to 1.6 GeV energy. We have done the shift according to three various reactions for protons, for which we have found experimental cross sections at 1.6 and 2.52 GeV energies. We have determined average ratio between the cross sections (1.6 GeV / 2.52 GeV). With this ratio we have shifted the cross sections and calculated deuteron beam intensity for the 1.6 GeV experiment. For some of the reactions, the beam intensity values were close to the intensity value determined by ^{24}Na, but some of them were one order of magnitude higher or lower, e.g., at ^{48}Sc or ^{57}Ni. No serious reason for the discrepancy was found, but we think the problem can be in unidentified contribution of another isotope to the same gamma line or in low statistics of measured gamma line, both during cross-section calculation from the 2.52 GeV experiment and/or during its use in the 1.6 GeV experiment. The final result (average over 10 reactions) is $(2.24 \pm 0.08) \cdot 10^{13}$ deuterons in the beam (value determined from the ^{24}Na is $(2.45 \pm 0.04) \cdot 10^{13}$, so this procedure gives rather good results, but is less reliable (Table 5).

Number of Deuterons Out of the Target. In the 1.6 GeV deuteron experiment we also used two circular copper foils placed in front of the target to measure exactly how many deuterons went out from the target. We used circles with 84 mm in diameter (the same as the target) and 120 mm in diameter. For the gamma measurement, we bended the foils to a smaller pieces approximately $25 \times 25 \times 3$ mm in size. Further analysis procedure was the same as at the front beam monitor. Weighted averages over the yields were normalized to the smaller foil. The results can be seen in Fig. 6.

Table 5. Summarized beam parameters for deuteron beams*. Uncertainties in X and Y shifts are assessed to be ± 2 mm (± 1 mm from the placement of the samples and ± 1 mm from the analysis)

Deuteron beam energy, GeV	1.6		2.52	
	V. Wagner	I. Zhuk	V. Wagner	I. Zhuk
X-axis shift, cm	−0.9	−0.64		1.5
Y-axis shift, cm	−0.6	−0.39	−0.4	−0.3
FWHM in x, cm	3.5	2.87	1.7	1.63
FWHM in y, cm	2.8	1.92	2.3	1.56
Measured beam intensity, 10^{13} — V. Wagner	2.4 ± 0.2**		0.642 ± 0.017	
Measured beam intensity, 10^{13} — W. Westmeier	2.45 ± 0.1		0.650 ± 0.021	
Final beam intensity, 10^{13}	2.45 ± 0.1		0.645 ± 0.013	
Deuterons out of the target — V. Wagner	6%		–	
Deuterons out of the target — W. Westmeier	21.3%		1%	
Deuterons out of the target — I. Zhuk	0.3%		3%	
Final number of deuterons out of the target	0.3%		3%	

*Data of I. Zhuk and W. Westmeier comes from personal communication and internal collaboration reports.
**Value determined only from ^{22}Na and ^{7}Be reactions using the method proposed by J. Blocki [10].
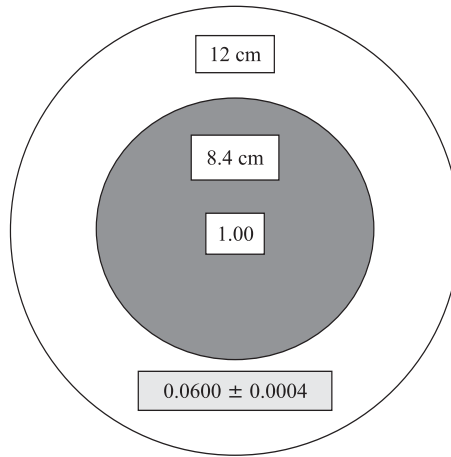
Fig. 6. Relative number of deuterons that did not hit the target during the 2.52 GeV deuteron experiment
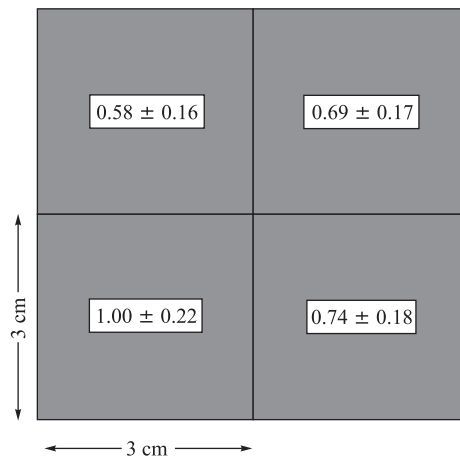
Fig. 7. Cu monitor for beam parallelism measurement

Beam Parallelism. In the 1.6 GeV experiment we placed a copper foil also behind the target to check the beam direction in the target (if the beam goes parallel with the target axis). We used foil with dimensions $60 \times 60 \times 0.12$ mm and made of the same copper as the front foil. After the irradiation we cut it onto 4 pieces of $30 \times 30 \times 0.12$ mm in size and measured each part separately. We detected the same isotopes as in the forward foil and were able to do the weighted

average over 4 gamma lines. From the results (Fig. 7), we can see that the beam was more or less parallel with the target axis during the 1.6 GeV deuteron run.

EXPERIMENTAL RESULTS

After the gamma-spectra evaluation and application of necessary spectroscopic corrections, we have determined the yields of produced isotopes (products of (n, xn) reactions). These yields are proportional to the neutron field in the place of the foil. We observed products with threshold energy (E_{thres}) from 5 to 60 MeV, which correspond to x from two up to nine. The yields (i.e., the number of activated nuclei per one gram of the foil and one deuteron beam) of observed isotopes are shown in the semilogarithmic scale in Figs. 8 and 9. The uncertainty bars in the graphs below are only from the Gauss fit in the DEIMOS32 and are hardly visible in the semilogarithmic scale (they are only a few %). Lines in the graphs are only to guide reader's eyes and have no real physical meaning.
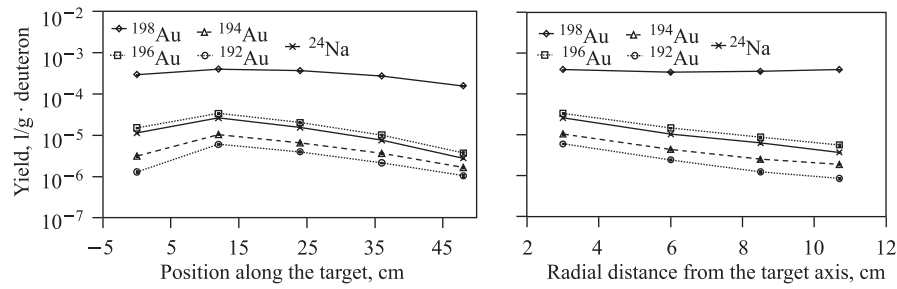
Fig. 8. Yields of observed isotopes in gold and aluminum foils — longitudinal direction 3 cm over the target axis (left) and in radial direction in the first gap of the setup (right), 1.6 GeV deuteron experiment
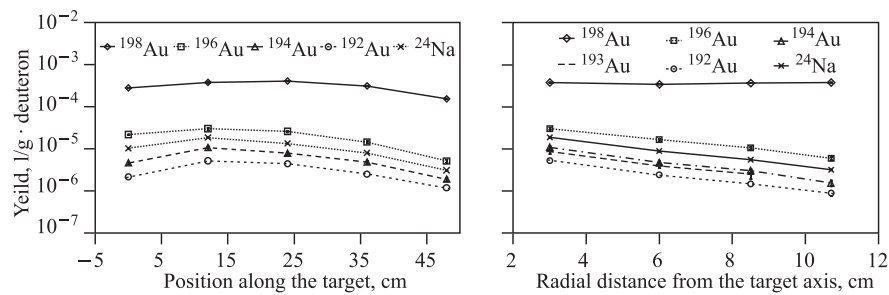
Fig. 9. Yields of observed isotopes in gold and aluminum foils — longitudinal direction 3 cm over the target axis (left) and in radial direction in the first gap of the setup (right), 2.52 GeV deuteron experiment

14

Products of the threshold reactions have their maxima near the first gap (~ 12 cm from the target beginning). This value does not differ very much in higher beam energies, although the deuteron range in the lead is rising. The reason is in the probability of the first collision (spallation), which takes place for the most of the deuterons in first ~ 20 cm of the target. During the spallation reaction high energy neutrons are produced mostly to the forward angles (intranuclear cascade), neutrons from high energy fission and evaporation are produced isotropicaly. These isotropicaly emitted neutrons cause most of the threshold reactions in the foils placed in front of the lead target.

Table 6. Yields of observed isotopes in Al and Au foils, the 1.6 GeV deuteron experiment at «E + T» setup

Foil	^{27}Al	^{197}Au				
Reaction	(n, α)	(n, γ)	$(n, 2n)$	$(n, 4n)$	$(n, 5n)$	$(n, 6n)$
Product	^{24}Na	^{198}Au	^{196}Au	^{194}Au	^{193}Au	^{192}Au
E_{thresh}, MeV	3.2	0	8.1	23.2	30.2	38.9
$T_{1/2}$, h	15	65	148	38	18	5
X, cm	Longitudinal yields for $R = 3.0$ cm [$10^{-6} \cdot \text{g}^{-1} \cdot \text{deuteron}^{-1}$]					
0.0	11.38(16)	296(5)	15.1(18)	3.15(14)	1.78(25)	1.30(5)
11.8	26.2(3)	400(3)	33.7(12)	10.5(5)	9.5(5)	6.05(13)
24.0	15.58(19)	366.9(29)	20.3(7)	6.6(3)	5.5(5)	3.99(16)
36.2	7.56(12)	273(6)	10.2(4)	3.66(19)	4.0(3)	2.14(7)
48.4	2.80(13)	157.6(13)	3.71(24)	1.66(9)	1.72(18)	1.05(7)
X, cm	Longitudinal yields for $R = 6.0$ cm [$10^{-6} \cdot \text{g}^{-1} \cdot \text{deuteron}^{-1}$]					
0.0	5.27(9)	264(3)	7.68(11)	1.61(4)	0.84(13)	0.81(5)
11.8	10.49(15)	343(6)	14.9(17)	4.43(17)	3.1(4)	2.46(9)
24.0	7.44(11)	327.4(20)	10.8(4)	3.48(15)	2.13(29)	1.84(7)
36.2	3.72(7)	256(6)	5.86(12)	1.93(6)	1.50(28)	1.16(8)
48.4	1.68(3)	146.6(24)	2.33(9)	0.89(6)	0.46(12)	0.75(11)
X, cm	Longitudinal yields for $R = 8.5$ cm [$10^{-6} \cdot \text{g}^{-1} \cdot \text{deuteron}^{-1}$]					
0.0	3.23(6)	277(4)	4.67(13)	1.01(5)	0.82(21)	0.46(9)
11.8	6.4(6)	359.6(25)	8.8(5)	2.54(15)	1.53(22)	1.25(7)
24.0	4.64(9)	335.6(28)	6.11(29)	1.99(12)	1.53(25)	1.09(6)
36.2	2.40(5)	290.8(22)	3.50(11)	1.27(5)	0.66(15)	0.73(10)
48.4	1.04(3)	176.5(11)	1.46(8)	0.61(4)	0.56(16)	0.56(22)
X, cm	Longitudinal yields for $R = 10.7$ cm [$10^{-6} \cdot \text{g}^{-1} \cdot \text{deuteron}^{-1}$]					
0.0	1.94(4)	302.2(28)	2.94(9)	0.76(4)	0.57(13)	0.29(7)
11.8	3.75(7)	398.2(28)	5.7(3)	1.90(11)	1.3(3)	0.86(5)
24.0	2.90(6)	349(11)	4.3(3)	1.34(13)	0.9(4)	0.69(5)
36.2	1.55(4)	352(3)	2.53(9)	0.93(4)	0.55(16)	0.46(10)
48.4	0.725(20)	210(3)	1.12(10)	0.39(5)	0.36(12)	0.34(12)

Table 7. Yields of observed isotopes in Al and Au foils, the 2.52 GeV deuteron experiment at «E + T» setup

Foil	^{27}Al	^{197}Au				
Reaction	(n, α)	(n, γ)	$(n, 2n)$	$(n, 4n)$	$(n, 5n)$	$(n, 6n)$
Product	^{24}Na	^{198}Au	^{196}Au	^{194}Au	^{193}Au	^{192}Au
E_{thresh}, MeV	3.2	0	8.1	23.2	30.2	38.9
$T_{1/2}$, h	15	65	148	38	18	5
X, cm	Longitudinal yields for $R = 3.0$ cm [$10^{-6} \cdot \text{g}^{-1} \cdot \text{deuteron}^{-1}$]					
0.0	11.63(21)	284(8)	22.3(4)	4.87(16)	2.3(4)	2.18(14)
11.8	20.8(29)	382(4)	35(4)	10.65(18)	8(1)	5.25(23)
24.0	15.08(28)	412.5(28)	20(5)	6.4(9)	6.8(8)	4.47(28)
36.2	8.94(15)	316(117)	14.9(3)	4.77(19)	5.6(5)	2.54(12)
48.4	3.46(8)	157(22)	5.59(11)	2.12(14)	2.11(29)	1.20(12)
X, cm	Longitudinal yields for $R = 6.0$ cm [$10^{-6} \cdot \text{g}^{-1} \cdot \text{deuteron}^{-1}$]					
0.0	5.14(28)	266.5(23)	9.84(28)	2(1)	2.3(7)	–
11.8	10.21(24)	343.8(18)	17.21(20)	5.16(24)	3.8(5)	2.39(17)
24.0	7.63(15)	342.5(18)	12.84(15)	4.2(26)	2.5(5)	3.0(4)
36.2	6.02(14)	269(13)	7.48(17)	2(3)	1.5(5)	–
48.4	1.9(3)	157.87(15)	3.26(17)	1.2(17)	0.82(27)	–
X, cm	Longitudinal yields for $R = 8.5$ cm [$10^{-6} \cdot \text{g}^{-1} \cdot \text{deuteron}^{-1}$]					
0.0	3.9(14)	265(8)	6.7(7)	1.4(11)	–	–
11.8	6.13(14)	368.7(12)	10.45(19)	3.33(14)	2.3(6)	1.48(12)
24.0	4.54(12)	350.7(23)	7.76(18)	2.4(19)	1.1(5)	1.3(4)
36.2	2.94(9)	291(7)	5.14(28)	1.6(10)	1.8(5)	–
48.4	1.23(6)	171.0(18)	2.08(14)	0.85(11)	–	–
X, cm	Longitudinal yields for $R = 10.7$ cm [$10^{-6} \cdot \text{g}^{-1} \cdot \text{deuteron}^{-1}$]					
0.0	2.09(8)	303.0(21)	3.82(22)	1.2(14)	–	–
11.8	3.56(17)	382(6)	6.43(18)	1.90(26)	–	0.80(12)
24.0	2.7(38)	382(56)	5.06(21)	1.8(10)	–	–
36.2	1.98(5)	340(6)	3.39(16)	1.0(6)	–	–
48.4	0.88(3)	209.4(15)	1.25(10)	0.64(28)	–	–

The nonthreshold ^{197}Au$(n, \gamma)^{198}$Au reaction is caused by the epithermal and resonance neutrons coming from the biological shielding. High energy neutrons escaping from the target and blanket are moderated in the polyethylene inside the shielding and some of them are backscattered into the inner volume of the biological shielding. Cadmium layer on the inner walls of the shielding absorbs only neutrons with energies under the cadmium cutoff (0.5 eV). Neutrons with higher energies create inside the biological shielding almost constant field.

In radial direction the yields of threshold reactions are quickly (almost exponentially) decreasing. From the product of nonthreshold reaction leading to

Table 8. Yields of observed isotopes in Bi foils, the 1.6 GeV deuteron experiment at «E + T» setup

Foil	^{209}Bi					
Reaction	$(n, 4n)$	$(n, 5n)$	$(n, 6n)$	$(n, 7n)$	$(n, 8n)$	$(n, 9n)$
Product	^{206}Bi	^{205}Bi	^{204}Bi	^{203}Bi	^{202}Bi	^{201}Bi
E_{thresh}, MeV	22.6	29.6	38.1	45.2	54	61.4
$T_{1/2}$, h	150	367	11	12	2	2
X, cm	Longitudinal yields for $R = 3.0$ cm [$10^{-6} \cdot$ g$^{-1} \cdot$ deuteron^{-1}]					
0.0	4.7(3)	5.3(29)	2.07(6)	1.23(19)	1.79(22)	1.7(3)
11.8	14.6(12)	17(14)	7.0(15)	6.3(12)	6.06(18)	3.4(4)
24.0	7.7(4)	11(5)	4.2(4)	3.41(13)	3.68(15)	2.7(3)
36.2	4.5(3)	4.9(24)	2.5(3)	2.01(19)	2.42(15)	1.81(17)
48.4	1.66(17)	2.1(19)	1.01(3)	0.93(5)	0.99(13)	0.55(6)
R, cm	Radial yields for $X = 11.8$ cm [$10^{-6} \cdot$ g$^{-1} \cdot$ deuteron^{-1}]					
3.0	14.6(12)	17(14)	7.0(15)	6.3(12)	6.06(18)	3.4(4)
6.0	4.87(20)	4.8(10)	2.17(5)	1.77(22)	1.54(8)	0.95(9)
8.5	2.41(14)	2.03(22)	0.937(25)	0.76(7)	0.67(4)	0.34(4)
10.7	1.36(10)	1.36(15)	0.539(16)	0.49(13)	0.350(20)	0.196(27)

Table 9. Yields of observed isotopes in Bi foils, the 2.52 GeV deuteron experiment at «E + T» setup

Foil	^{209}Bi					
Reaction	$(n, 4n)$	$(n, 5n)$	$(n, 6n)$	$(n, 7n)$	$(n, 8n)$	$(n, 9n)$
Product	^{206}Bi	^{205}Bi	^{204}Bi	^{203}Bi	^{202}Bi	^{201}Bi
E_{thresh}, MeV	22.6	29.6	38.1	45.2	54	61.4
$T_{1/2}$, h	150	367	11	12	2	2
X, cm	Longitudinal yields for $R = 3.0$ cm [$10^{-6} \cdot$ g$^{-1} \cdot$ deuteron^{-1}]					
0.0	11.7(13)	9.5(11)	5.4(4)	4.28(28)	7.99(29)	3.9(8)
11.8	30(4)	27.6(21)	17(24)	16.5(13)	13.0(4)	8.9(9)
24.0	12.1(10)	10.8(13)	6.2(7)	5.4(5)	5.66(25)	2.6(3)
36.2	5.1(4)	6(6)	2.7(7)	2.4(7)	2.68(11)	1.75(24)
48.4	2.3(4)	4(3)	1.29(27)	1.6(6)	1.49(21)	0.58(14)
R, cm	Radial yields for $X = 11.8$ cm [$10^{-6} \cdot$ g$^{-1} \cdot$ deuteron^{-1}]					
3.0	30(4)	27.6(21)	17(24)	16.5(13)	13.0(4)	8.9(9)
6.0	8.6(5)	7.6(13)	4.1(17)	3.11(16)	2.73(20)	1.35(20)
8.5	4.07(21)	4(4)	2.05(24)	1.51(6)	1.098(22)	0.70(7)
10.7	2.30(6)	1.99(29)	0.9(3)	0.81(17)	0.57(6)	0.30(4)

Table 10. Yields of observed isotopes in In foils, the 1.6 GeV deuteron experiment at «E + T» setup

Foil	^{115}In						
Reaction	(n,γ)	(n,n')	$(n,2n)$	$(n,3n)$	$(n,5n)$	$(n,6n)$	$(n,7n)$
Product	^{116m}In	^{115m}In	^{114m}In	^{113m}In	^{111}In	^{110}In	^{109}In
E_{thresh}, MeV	0	0.4	9.1	16.4	33.7	43.8	51.2
$T_{1/2}$, h	1	4.5	1188	1.7	2.8	4.9	4.2
X, cm	Longitudinal yields for $R = 3.0$ cm $[10^{-6}\cdot\text{g}^{-1}\cdot\text{deuteron}^{-1}]$						
0.0	440(16)	54.2(7)	419(44)	2.86(17)	3.5(18)	1.10(21)	0.70(7)
11.8	741(5)	152.9(17)	296(62)	9.2(4)	15.0(9)	4.6(3)	3.52(24)
24.0	715(4)	83.4(12)	147(41)	4.36(21)	9.9(6)	2.14(23)	2.13(14)
36.2	446.8(25)	49.8(7)	96(23)	2.47(14)	6.7(4)	1.06(16)	1.12(7)
48.4	222.7(17)	11.91(29)	31(12)	–	1.80(16)	0.62(9)	0.55(6)
R, cm	Radial yields for $X = 11.8$ cm $[10^{-6}\cdot\text{g}^{-1}\cdot\text{deuteron}^{-1}]$						
3.0	741(5)	152.9(17)	296(62)	9.2(4)	15.0(9)	4.6(3)	3.52(24)
6.0	747(4)	67.4(9)	594(521)	3.8(2)	5.9(5)	1.88(21)	0.75(11)
8.5	751(4)	44.1(7)	–	1.90(14)	2.2(15)	1.54(26)	0.56(14)
11.5	959(5)	24.6(6)	51(61)	1.05(16)	2.3(5)	0.62(24)	–

Table 11. Yields of observed isotopes in In foils, the 2.52 GeV deuteron experiment at «E + T» setup

Foil	^{115}In						
Reaction	(n,γ)	(n,n')	$(n,2n)$	$(n,3n)$	$(n,5n)$	$(n,6n)$	$(n,7n)$
Product	^{116m}In	^{115m}In	^{114m}In	^{113m}In	^{111}In	^{110}In	^{109}In
E_{thresh}, MeV	0	0.4	9.1	16.4	33.7	43.8	51.2
$T_{1/2}$, h	1	4.5	1188	1.7	2.8	4.9	4.2
X, cm	Longitudinal yields for $R = 3.0$ cm $[10^{-6}\cdot\text{g}^{-1}\cdot\text{deuteron}^{-1}]$						
0.0	580(30)	107.7(13)	69.5(29)	5.3(5)	7.7(5)	1.88(14)	1.80(12)
11.8	950(30)	234.9(28)	140(40)	13.0(5)	22.1(14)	6(3)	6.48(21)
24.0	953(28)	119.6(13)	74.9(16)	6.5(5)	9.3(4)	2.49(19)	2.65(18)
R, cm	Radial yields for $X = 11.8$ cm $[10^{-6}\cdot\text{g}^{-1}\cdot\text{deuteron}^{-1}]$						
3.0	950(30)	234.9(28)	140(40)	13.0(5)	22.1(14)	6(3)	6.48(21)
6.0	920(40)	117.0(14)	56(4)	5.8(5)	6.06(22)	2.1(6)	1.81(18)
8.5	910(40)	63.7(10)	46.1(25)	3.3(3)	2.90(9)	0.6(4)	0.45(8)
11.5	1110(40)	38.0(8)	39(14)	1.8(3)	1.43(8)	–	0.35(8)

Table 12. Yields of observed isotopes in Ta foils, the 1.6 GeV deuteron experiment at «E + T» setup

Foil	^{181}Ta					
Reaction	(n, γ)	$(n, 2n)$	$(n, 4n)$	$(n, 5n)$	$(n, 6n)$	$(n, 7n)$
Product	^{182}Ta	^{180}Ta	^{178m}Ta	^{177}Ta	^{176}Ta	^{175}Ta
E_{thresh}, MeV	0	7.6	22.7	29.2	37.5	44.5
$T_{1/2}$, h	2746	8	2	57	8	11
X, cm	Longitudinal yields for $R = 3.0$ cm [$10^{-6} \cdot \text{g}^{-1} \cdot \text{deuteron}^{-1}$]					
0.0	162(32)	12.8(15)	1.9(7)	0.24(3)	1.2(5)	0.88(20)
11.8	517(234)	46(12)	4.7(4)	1.38(14)	5.84(25)	5.43(22)
24.0	263(62)	17.2(9)	1.92(23)	0.49(6)	2.56(12)	2.5(5)
36.2	151(27)	7.8(10)	0.98(19)	0.28(3)	1.23(7)	1.07(10)
48.4	78(21)	3.23(27)	0.51(14)	0.144(18)	0.64(4)	0.61(7)
X, cm	Longitudinal yields for $R = 6.0$ cm [$10^{-6} \cdot \text{g}^{-1} \cdot \text{deuteron}^{-1}$]					
0.0	309(14)	10.2(6)	–	0.121(19)	0.87(15)	0.70(6)
11.8	215(14)	9.8(5)	1.001(18)	0.309(26)	1.36(6)	1.11(13)
24.0	149(10)	36.1(16)	–	0.196(14)	6.01(20)	2.93(19)
36.2	259(9)	2.7(3)	–	0.207(19)	0.89(13)	0.76(28)
48.4	84.7(17)	1.09(24)	–	0.053(8)	0.40(7)	0.4(4)
X, cm	Longitudinal yields for $R = 8.5$ cm [$10^{-6} \cdot \text{g}^{-1} \cdot \text{deuteron}^{-1}$]					
0.0	337(7)	7.2(19)	–	0.298(18)	1.15(13)	0.42(5)
11.8	444(24)	13.8(8)	1.51(3)	0.36(5)	1.95(8)	1.37(23)
24.0	144(7)	23.7(10)	–	0.118(13)	3.79(13)	1.93(15)
36.2	185(7)	1.12(20)	–	0.149(11)	0.28(10)	0.277(25)
48.4	85(3)	0.7(6)	–	0.066(6)	0.28(6)	0.22(5)
X, cm	Longitudinal yields for $R = 10.7$ cm [$10^{-6} \cdot \text{g}^{-1} \cdot \text{deuteron}^{-1}$]					
0.0	282(6)	3.6(5)	–	0.215(16)	–	–
11.8	461(12)	9.0(4)	1.136(25)	0.27(3)	1.03(5)	0.85(27)
24.0	264(8)	29.0(17)	–	0.097(27)	4.07(19)	2.11(35)
36.2	268(8)	1.29(20)	–	0.163(11)	–	0.21(3)
48.4	97(3)	0.64(18)	–	0.073(6)	–	0.095(14)

Table 13. Yields of observed isotopes in Ta foils, the 2.52 GeV deuteron experiment at «E + T» setup

Foil	^{181}Ta					
Reaction	(n,γ)	$(n,2n)$	$(n,4n)$	$(n,5n)$	$(n,6n)$	$(n,7n)$
Product	^{182}Ta	^{180}Ta	^{178m}Ta	^{177}Ta	^{176}Ta	^{175}Ta
E_{thresh}, MeV	0	7.6	22.7	29.2	37.5	44.5
$T_{1/2}$, h	2746	8	2	57	8	11
X, cm	Longitudinal yields for $R = 3.0$ cm [$10^{-6} \cdot \mathrm{g}^{-1} \cdot \mathrm{deuteron}^{-1}$]					
0.0	190(7)	32.2(22)	2.52(8)	8.9(12)	3.2(4)	1.53(23)
11.8	319(5)	46(3)	4.31(7)	11.4(8)	5.5(5)	3.5(4)
24.0	321(15)	29.7(14)	3.10(14)	21.3(11)	4.0(4)	2.69(23)
36.2	236(13)	16.8(11)	1.87(28)	15.2(12)	2.5(3)	1.82(25)
48.4	108(3)	6.4(6)	0.89(16)	11(3)	0.90(20)	1.0(9)
X, cm	Longitudinal yields for $R = 6.0$ cm [$10^{-6} \cdot \mathrm{g}^{-1} \cdot \mathrm{deuteron}^{-1}$]					
0.0	164.5(28)	10.1(25)	–	318(35)	–	0.45(15)
11.8	247(12)	16.8(10)	2.06(7)	22.9(22)	2.3(4)	1.7(4)
24.0	284(6)	9.9(20)	–	74.2(28)	2.3(5)	1.3(4)
36.2	224(4)	5.2(19)	–	141(6)	1.0(4)	0.83(13)
48.4	100(3)	4.5(12)	–	178(29)	–	0.42(10)
X, cm	Longitudinal yields for $R = 8.54$ cm [$10^{-6} \cdot \mathrm{g}^{-1} \cdot \mathrm{deuteron}^{-1}$]					
0.0	175(5)	10.2(20)	–	–	–	–
11.8	260(8)	11.1(5)	1.30(4)	21.9(16)	1.50(29)	0.87(8)
24.0	275(6)	–	–	96(25)	1.14(29)	0.99(13)
36.2	217(5)	4.8(11)	–	598(25)	1.0(4)	0.55(20)
48.4	102(3)	4.4(15)	–	180(21)	0.59(23)	–
X, cm	Longitudinal yields for $R = 10.7$ cm [$10^{-6} \cdot \mathrm{g}^{-1} \cdot \mathrm{deuteron}^{-1}$]					
0.0	180(4)	6.5(18)	–	256(16)	–	–
11.8	308(81)	9.8(19)	0.91(5)	24.3(11)	1.21(18)	0.80(15)
24.0	274(8)	–	–	129(5)	–	0.44(20)
36.2	231(7)	3.0(10)	–	213(9)	–	0.46(8)
48.4	149(13)	–	–	176(13)	–	–

Table 14. Yields of observed isotopes in Y foils, the 1.6 GeV deuteron experiment at «E + T» setup

Foil	^{89}Y				
Reaction	(n, γ)	$(n, 2n)$	$(n, 3n)$	$(n, 4n)$	$(n, 5n)$
Product	^{90m}Y	^{88}Y	^{87}Y	^{86}Y	^{85}Y
E_{thresh}, MeV	0	11.6	21.1	33	42.6
$T_{1/2}$, h	3	2568	80	15	3
X, cm	Longitudinal yields for $R = 0.0$ cm [$10^{-6} \cdot \mathrm{g}^{-1} \cdot \mathrm{deuteron}^{-1}$]				
0.0	0.29(4)	77.7(12)	54.2(5)	22.8(22)	7.3(11)
11.8	0.79(5)	145.3(17)	103.0(22)	40(3)	11.8(13)
24.0	0.480(23)	67.6(11)	50.2(6)	18.1(15)	5.8(8)
36.2	0.238(25)	27.5(6)	20.95(29)	8.2(5)	2.06(5)
48.4	0.070(5)	9.1(3)	7.08(15)	2.64(8)	0.80(13)
X, cm	Longitudinal yields for $R = 3.0$ cm [$10^{-6} \cdot \mathrm{g}^{-1} \cdot \mathrm{deuteron}^{-1}$]				
0.0	0.196(9)	19.8(6)	8.84(20)	2.21(5)	0.500(19)
11.8	0.514(14)	47.7(8)	30.1(5)	9.35(21)	2.5(4)
24.0	0.347(10)	26.6(8)	18.04(20)	5.80(16)	1.2(3)
36.2	0.193(7)	13.9(4)	9.61(15)	3.27(12)	0.48(6)
48.4	0.051(4)	4.78(22)	4.01(5)	1.44(11)	0.196(15)
X, cm	Longitudinal yields for $R = 6.0$ cm [$10^{-6} \cdot \mathrm{g}^{-1} \cdot \mathrm{deuteron}^{-1}$]				
0.0	5.4(13)	–	3.60(5)	0.983(26)	–
11.8	0.311(12)	–	5.8(3)	3.01(6)	0.651(24)
24.0	0.28(7)	–	5.32(12)	2.64(8)	0.75(5)
36.2	41(5)	7.64(12)	4.9(3)	1.6(3)	–
48.4	110(17)	3.40(8)	2.49(8)	0.92(5)	130(99)
X, cm	Longitudinal yields for $R = 8.5$ cm [$10^{-6} \cdot \mathrm{g}^{-1} \cdot \mathrm{deuteron}^{-1}$]				
0.0	6.4(13)	–	2.39(7)	0.62(6)	–
11.8	0.242(26)	–	3.68(25)	1.82(5)	0.431(23)
24.0	0.23(6)	–	3.29(9)	1.51(4)	0.42(3)
36.2	56(7)	4.66(12)	2.97(15)	0.94(3)	–
48.4	196(21)	2.00(5)	1.38(4)	0.480(21)	–
X, cm	Longitudinal yields for $R = 10.5$ cm [$10^{-6} \cdot \mathrm{g}^{-1} \cdot \mathrm{deuteron}^{-1}$]				
0.0	10.6(8)	–	1.612(25)	0.442(18)	–
11.8	0.17(3)	7.39(28)	2.36(21)	1.14(9)	0.241(13)
24.0	0.19(7)	–	2.17(6)	1.056(28)	0.301(22)
36.2	82(8)	3.27(9)	2.03(9)	0.610(24)	–
48.4	287(28)	1.52(4)	2.49(8)	0.342(24)	–

Table 14. Continuation

X, cm	Longitudinal yields for $R = 13.5$ cm [$10^{-6} \cdot$g$^{-1} \cdot$deuteron^{-1}]				
0.0	14.9(12)	–	1.00(3)	0.270(16)	–
11.8	0.099(21)	4.36(24)	2.1(6)	0.66(5)	0.139(9)
24.0	0.10(6)	–	1.19(4)	0.601(18)	0.165(21)
36.2	170(11)	1.80(9)	1.23(4)	0.358(17)	–
48.4	614(48)	0.96(5)	0.65(4)	0.20(3)	–

Table 15. Yields of observed isotopes in Y foils, the 2.52 GeV deuteron experiment at «E + T» setup

Foil	^{89}Y				
Reaction	(n,γ)	$(n,2n)$	$(n,3n)$	$(n,4n)$	$(n,5n)$
Product	^{90m}Y	^{88}Y	^{87}Y	^{86}Y	^{85}Y
E_{thresh}, MeV	0	11.5	20.8	32.7	42.1
$T_{1/2}$, [h]	3	2568	80	15	3
X, cm	Longitudinal yields for $R = 3.0$ cm [$10^{-6} \cdot$g$^{-1} \cdot$deuteron^{-1}]				
0.0	0.196(18)	16.7(13)	6.01(13)	2.14(18)	0.44(12)
11.8	0.56(6)	36.8(24)	21.47(12)	6.7(6)	1.6(5)
24.0	0.43(4)	33.4(18)	16.95(27)	6.27(18)	2(2)
36.2	0.213(22)	19.0(20)	10.24(16)	3.99(27)	1.08(9)
48.4	–	6.6(8)	4.69(10)	2.20(18)	0.5(3)
R, cm	Radial yields for $X = 11.8$ cm [$10^{-6} \cdot$g$^{-1} \cdot$deuteron^{-1}]				
3.0	0.56(6)	36.8(24)	21.47(29)	6.7(6)	1.6(5)
6.0	0.360(24)	21.0(15)	10.91(18)	3.01(27)	0.7(7)
8.5	0.256(21)	12.0(10)	6.36(12)	1.8(3)	0.38(18)
10.7	0.182(23)	8(1)	3.30(9)	1.14(10)	0.196(29)

^{198}Au, it can be seen, that the epithermal and resonance neutron field is really homogeneous in radial direction (Table 6).

The threshold energies of the reactions were overtaken from [14]. The half-lives of the isotopes were taken from [15] and have rounded values.

Longitudinal ratios between yields at the end of the target ($X = 48$ cm) and in front of the target ($X = 0$ cm) as a function of reaction threshold energy are shown in Figs. 10 and 11. Neither in the 1.6 GeV deuteron experiment nor in the 2.52 GeV deuteron experiment a clear dependence is visible like it was during proton experiments (see, e.g., [1]). There is some trend that shows a decrease of the ratio with rising threshold energy, that means the difference in neutron flux in front of and behind the target is smaller for neutron energies higher than ~ 20 MeV.
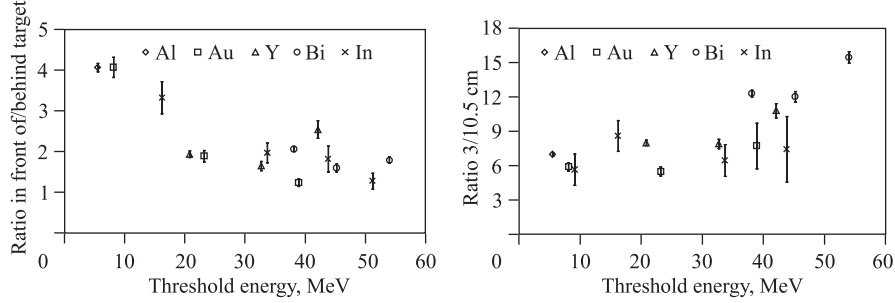
Fig. 10. Ratios of yields at the end of the target ($X = 48$ cm) and in front of the target ($X = 0$ cm) as a function of threshold energy (left). Ratios of yields at $R = 10.7$ cm and at $R = 3$ cm as a function of threshold energy (right). The 1.6 GeV deuteron experiment
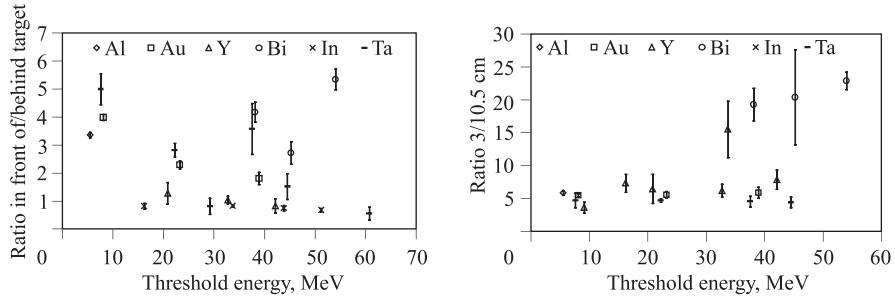
Fig. 11. Ratios of yields at the end of the target ($X = 48$ cm) and in front of the target ($X = 0$ cm) as a function of threshold energy (left). Ratios of yields at $R = 10.7$ cm and at $R = 3$ cm as a function of threshold energy (right). The 2.52 GeV deuteron experiment

The difference comes from the probability of the first interaction, respectively spallation reaction. Neutron field inside the setup is a complicated mixture of spallation, fission, moderated and back-scattered neutrons. Neutron field has its maximum around 12 cm from the target beginning (see, e.g., Fig. 8). Neutrons with higher energies come from the intranuclear phase of the spallation reaction and are emitted more forward, in contradiction to neutrons below 20 MeV, which come from evaporation and fission phase of the spallation reaction and are emitted isotropicaly. Epithermal and resonance neutrons come from the biological shielding. Combination of the spallation probability and various sources of neutrons in spallation reaction causes observed difference in front/end yield ratio for threshold energy of approximately 20 MeV.

In the radial direction ratios between yields at $R = 3$ cm and $R = 10.7$ cm are shown (Fig. 10 and Fig. 11). Ratios are made of the foils placed in the first gap of the setup (place with maximal neutron flux). The ratios oscillate around

23
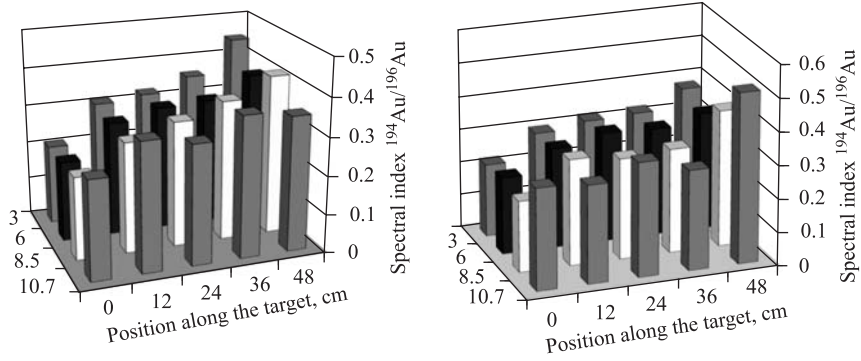
Fig. 12. Neutron spectra hardening along the target in the 1.6 GeV (left) and 2.52 GeV (right) deuteron experiments (ratio between ^{194}Au and ^{196}Au)
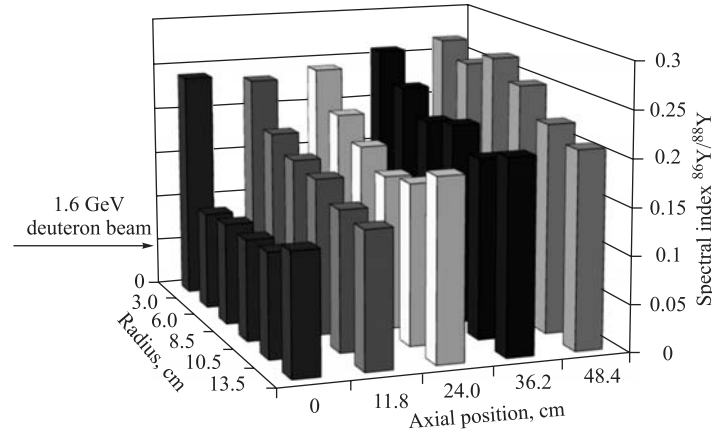
Fig. 13. Neutron spectra hardening along the target in the 1.6 GeV deuteron experiments (ratio between ^{86}Y and ^{88}Y). Almost constant ratio at zero cm radius is caused by the beam

the value 6.5 up to the neutron energy 35 MeV. Above 35 MeV there is a steep increase. This difference originates from the course of spallation reaction — neutrons with higher energies are produced mainly in intranuclear cascade and move to forward angles, so they can hardly get far from the target in radial direction.

Spectral Indexes. We have compared yields of reactions with different thresholds (^{194}Au/^{196}Au and ^{192}Au/^{196}Au, respectively ^{86}Y/^{88}Y). We have observed a spectrum hardening at the end of the target (see Fig. 12 and Fig. 13). Fig. 12 and Fig. 13 are, in principal, similar to the previous Fig. 10 and Fig. 11. The threshold energy is here hidden in the ratio of two reactions with different thresholds. The

24
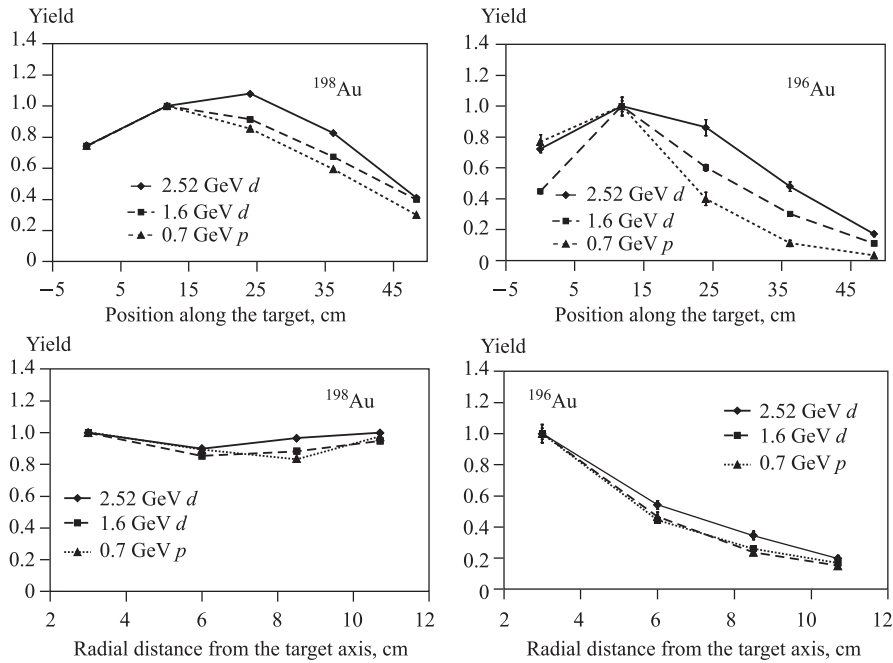
Fig. 14. Comparison between 0.7 GeV proton and two deuteron experiments, yields normalized to the second foil in longitudinal direction, respectively to the first foil in radial direction

observed spectrum hardening is specific for the spallation reaction; high energy neutrons are produced more into the forward direction.

Comparison between experimental results of various «E + T» experiments (nonthreshold and threshold yields per 1 gram of foil material and one beam particle) are shown in Fig. 14. The data are normalized to the second foil to see the difference in the shape. The increase in the neutron flux can be seen behind the first gap (its maximum) with rising beam energy.

COMPARISON WITH MCNPX SIMULATIONS

For the both «E + T» deuteron experiments we made a set of MCNPX calculations. We used version 2.7.a. In the input file, we described the complex geometry of the uranium rod blanket, the segmented lead target, the polyethylene shielding, all metal frames, shells, and support structures; for more details see Fig. 15 or [7].

25
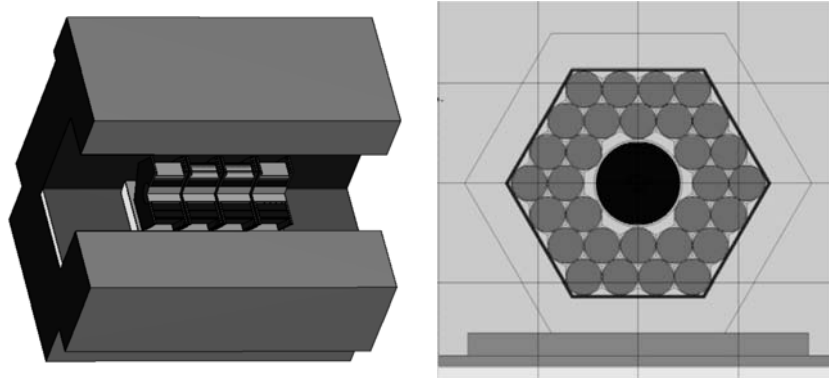
Fig. 15. Visualization of the «Energy plus Transmutation» setup as defined in MCNPX input file. On the left is SABRINA [16] plot provided by Jaroslav Šolc
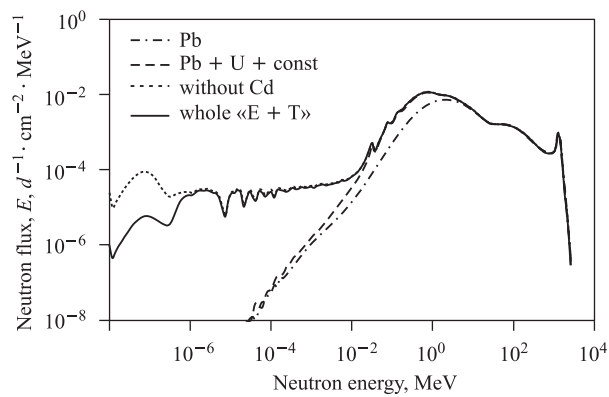
Fig. 16. Setup parts influence on the neutron field in the fourth target part

The simulated deuteron beams had energy of 1.6 GeV and 2.52 GeV and Gaussian profile, values of their horizontal and vertical FWHM and shift were the same as those measured in the experiment. Simulations were computed primarily using the INCL/ABLA model. The other available combinations of models were also tested.

Advantage of the MCNPX simulation is a possibility of easy calculation of practically immeasurable things. We have tested the influence of various parts of the «E + T» setup on produced neutron field. Results of the calculations can be seen in Fig. 16. Addition of natural uranium (and support structures) to the bare lead target causes more neutrons in the region between 1 keV and 1 MeV due to the high energy fission. Biological shielding adds further neutrons to the

26

low energy region below 10 keV and also the second maximum of the neutron spectrum around 0.025 eV. Addition of the cadmium layer on the inner walls of the biological shielding suppresses this thermal energy peak. In all cases, a small peak can be seen close to the highest neutron energies. These neutrons come from the deuteron disintegration.

Absorptions on the resonances in ^{238}U are also visible in Fig. 16. First depression in the low energy part of the neutron spectrum corresponds to the first important resonance in ^{238}U$(n,\gamma)^{239}$U reaction at 6.67 eV.

Nonthreshold reactions can be calculated directly using f4+fm tally. For threshold reactions the situation is more complicated because of the missing cross sections. Products of some (n, xn) reactions can be also calculated with f4+fm tally, but the MCNPX handles with cross sections not ideally. It uses libraries up to their highest energy, then when it has no model, it takes the last value in library and uses it for the convolution with the rest of the neutron spectrum. In reality, (n, xn) cross sections decrease slightly after their peak, so this approach is not suitable. We solved this problem in the following way.

We add small volumes to the «E + T» model correspondent to the specific detector positions during each irradiation and calculate the neutron, proton, deuteron and charged pion fluxes in these volumes using the MCNPX. We calculate cross-sections of the (n, xn), (p, pxn), (d, dxn), and $(\pi, \pi xn)$ reactions in TALYS [17] and MCNPX and we connect them together. We make manual folding of the

Table 16. Contribution of various particles to the total yield, result of MCNPX simulation and manual folding. Positions in the first gap and behind the target, radial distance 3 cm and 10.7 cm, the 2.52 GeV deuteron experiment

First gap of the setup						
	^{196}Au		^{194}Au		^{192}Au	
	3 cm	10.7 cm	3 cm	10.7 cm	3 cm	10.7 cm
Neutrons	98.8%	99.7%	94.6%	98.7%	92.8%	98.2%
Protons	1.1%	0.26%	5.06%	1.14%	6.63%	1.53%
Deuterons	0.03%	0.05%	0.07%	0.08%	0.11%	0.07%
Charged pions	0.08%	0.02%	0.24%	0.08%	0.45%	0.16%
Behind the setup						
	^{196}Au		^{194}Au		^{192}Au	
	3 cm	10.7 cm	3 cm	10.7 cm	3 cm	10.7 cm
Neutrons	97.9%	99.2%	92.7%	97.3%	91.3%	96.6%
Protons	1.96%	0.70%	6.99%	2.51%	8.14%	3.05%
Deuterons	0.06%	0.02%	0.15%	0.06%	0.28%	0.12%
Charged pions	0.08%	0.05%	0.18%	0.12%	0.31%	0.21%

27
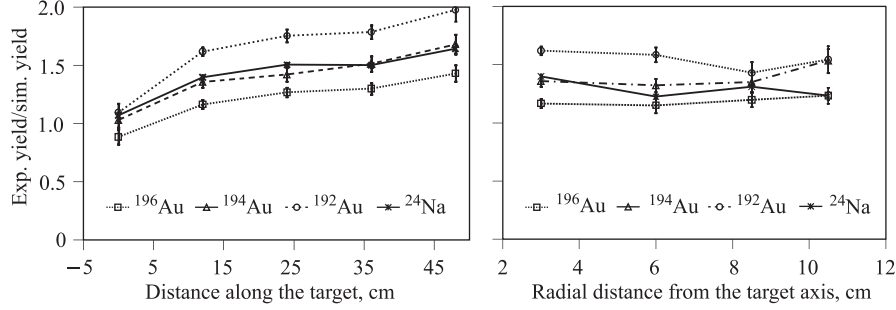
Fig. 17. Experiment versus simulation ratio of Au and Al yields, left — in longitudinal direction 3 cm over the axis, right — in radial direction in the first gap of the «E+T» setup, the 1.6 GeV deuteron experiment, INCL/ABLA models
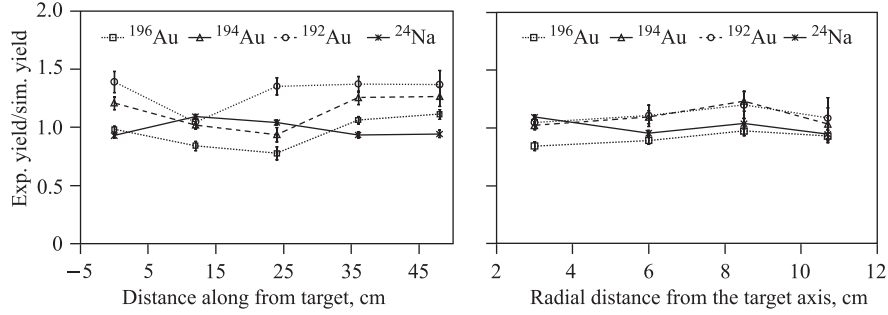
Fig. 18. Experiment versus simulation ratio of Au and Al yields, left — in longitudinal direction 3 cm over the axis, right — in radial direction in the first gap of the «E+T» setup, the 2.52 GeV deuteron experiment, INCL/ABLA models

fluxes and cross sections in Excel, according to the following equation:

$$N_{\text{yield}} = \frac{1}{A_r m_u} \int_0^{E_{\text{beam}}} [\phi_n(E) \cdot \sigma_n(E) + \phi_p(E) \cdot \sigma_p(E) + \phi_{pi}(E) \cdot \sigma_{pi}(E) + \\ + \phi_d(E) \cdot \sigma_d(E)] \, dE, \quad (3)$$

where A_r is the specific atomic mass of a chemical element from which the foil was made and m_u is the unified atomic mass unit. Final outputs from the simulation part are directly the yields of isotopes. Contributions of various particles to the total isotope production in gold during the 2.52 GeV deuteron experiment are displayed in the following Table 16 (result of MCNPX spectra simulation and manual folding). Most important is the contribution of neutrons, protons can create also a substantial part of the yield. Contribution of deuterons

28

and pions is under the level of neutron spectra uncertainty and could be thus negligible. Nevertheless deuterons and charged pions are always included.

Examples of the experiment to simulation ratios for the 1.6 and 2.52 GeV deuteron experiments are in the following Fig. 17 and Fig. 18. Lines between the points are only to lead reader's eyes. Uncertainty bars contain only statistical uncertainty from the DEIMOS32 and MCNPX, because the main purpose of this comparison is to see the relative differences between various isotopes and different measurement points (some uncertainties are the same for all points, e.g., beam intensity uncertainty, and their involvement would be misleading in this case).

If we look for the trends in the data it may be stated that the MCNPX simulation is in good qualitative agreement with the measured data. Absolute values of the ratio depend on the beam intensity determination. Any disagreement in radial direction was not observed, contrary to proton experiments with energies higher than 1.5 GeV.

Neutron Multiplicity. The so-called water-bath/activation foil method [18] is often used for the determination of the integral numbers of neutrons produced in thick targets. The conventional variant of this method uses two basic premises: neutrons from the source are predominantly contained within the moderator volume; and it is possible to integrate the measured thermal flux distribution over the water volume with adequate precision. As the latter requires the usage of a large-scale grid of activation foils, we have used a new form of this method [19], which replaces the flux integration by relating a small-scale set of foil activities to the integral quantity — the integral number of neutrons produced per one beam particle (the so-called neutron multiplicity) $n_{\text{total}}^{\text{sim}}$ obtained by simulation.

Polyethylene in the biological shielding of the «E + T» setup worked as a water bath — it moderated outgoing neutrons. We did not take into account front and back openings of the biological shielding. We did multiplicity simulations in MCNPX 2.7.a using various models. For calculation of the neutron multiplicity, we determined the ratios between experimental and simulated yields of ^{198}Au in all gold samples. We tried to use also tantalum samples for the first time, because tantalum has similar cross section for (n, γ) reaction as the gold has, and tantalum samples were placed close (or even at the same place) as the gold samples. We calculated weighted average over these ratios and we multiplied it with the simulated neutron multiplicity — see the following equation:

$$n_{\text{total}}^{\text{exp}} = n_{\text{total}}^{\text{sim}} \left\langle \frac{N_{\text{yield}}^{\text{exp}}}{N_{\text{yield}}^{\text{sim}}} \right\rangle. \tag{4}$$

The advantage of this procedure is that the experimental value of neutron multiplicity $n_{\text{total}}^{\text{exp}}$ is highly insensitive to the simulated value $n_{\text{total}}^{\text{sim}}$ and its uncertainty. Assuming that the MCNPX describes well the spatial distribution of the neutrons as well as the shape of low energy part of neutron spectrum and its

Table 17. Experimental neutron multiplicity in the «E + T» setup evaluated using various MCNPX models

	1.6 GeV		2.52 GeV	
Model	Au	Ta	Au	Ta
Bertini–Dresner	78.1	67.6	82.8	67.9
Bertini–Abla	88.8	80.3	95.9	82.0
CEM03	87.9	79.4	96.6	80.3
INCL–Abla	100.8	92.9	107.4	93.1
INCL–Dresner	100.3	92.6	107.8	94.1
Isabel–Abla	89.6	81.3	97.6	83.7
Isabel–Dresner	78.3	69.1	84.7	69.3
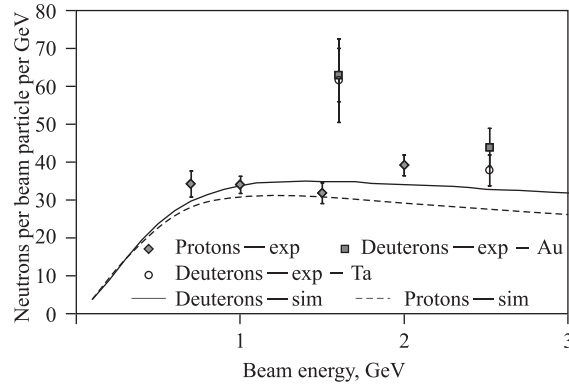
Fig. 19. Neutron multiplicities for the «E + T» setup normalized per GeV. Points are from the experiments, lines from the MCNPX simulation

approximate magnitude; the product of the two terms in equation (4) effectively cancels out the dependence on $n_{\text{total}}^{\text{sim}}$. Neutron multiplicity results for deuteron experiments are summarized in Table 17. Results from gold and tantalum samples are comparable within the uncertainties. Multiplicity determined by tantalum seems to be closer to the simulated multiplicity of the «E + T» setup, see Fig. 19.

CONCLUSIONS

We studied the neutron field produced in the experimental setup called «Energy plus Transmutation» by means of neutron activation detectors. The «E + T» setup consisted of thick lead target, the natural uranium blanket, and the surrounding polyethylene radiation shielding. The activation detectors had a form of thin foils made of aluminum, bismuth, indium, gold, tantalum, and yttrium.

Setup with the detectors was irradiated by 1.6 and 2.52 GeV deuterons from the Nuclotron accelerator with the total intensity 10^{13}. Special systems for beam monitoring were used to measure the beam shape, profile and total intensity.

We analyzed γ-ray spectra of activated detectors in order to get the yields of (n,γ), (n,xn), and (n,α) reactions. When evaluating the yields we included various spectroscopic corrections to control all possible sources of uncertainties. Finally, we compared the experimental yields of ^{198}Au, ^{196}Au, ^{194}Au, ^{192}Au, and ^{24}Na with the results of the MCNPX simulation. A good qualitative agreement was found between each other. The simulations follow quite well the trends of the measured data.

Polyethylene biological shielding in combination with nonthreshold reactions enabled us to calculate the total number of produced neutrons. In the case of deuteron experiments neutron multiplicity was up to 108 neutrons per one deuteron at the 2.52 GeV irradiation.

REFERENCES

1. *Krása A. et al.* Neutron Emission in the Spallation Reactions of 1 GeV Protons on a Thick Lead Target Surrounded by Uranium Blanket. JINR Preprint E15-2007-81. Dubna, 2007.

2. *Krása A. et al.* Neutron production in $p+$ Pb/U at 2 GeV. JINR Preprint E1-2009-195. Dubna, 2009.

3. *Krivopustov M. I. et al.* Investigation of Neutron Spectra and Transmutation of ^{129}I, ^{237}Np and Other Nuclides with 1.5 GeV Protons from the Dubna Nuclotron Using the Electronuclear Setup «Energy plus Transmutation». JINR Preprint E1-2004-79. Dubna, 2004.

4. *Svoboda O. et al.* Study of Spallation Reaction, Neutron Production and Transport in Thick Lead Target and Uranium Blanket Irradiated with 0.7 GeV Protons. JINR Preprint E15-2009-177. Dubna, 2009.

5. *Krivopustov M. I. et al.* First Experiments with a Large Uranium Blanket within the Installation «Energy plus Transmutation» Exposed to 1.5 GeV Protons // Kerntechnik. 2003. V. 68. P. 48.

6. MCNPX (Monte Carlo N-Particle eXtended). http://mcnpx.lanl.gov

7. *Majerle M. et al.* Monte Carlo Studies of the «Energy plus Transmutation» System. JINR Preprint E15-2007-82. Dubna, 2007.

8. *Frána J.* Program DEIMOS32 for Gamma-Ray Spectra Evaluation // J. Rad. Nucl. Chem. 2003. V. 257, No. 3 P. 583–587.

9. *Banaigs J. et al.* // Nucl. Instrum. Meth. Phys. Res. 1971. V. 95. P. 307–311.
10. *Blocki J. et al.* Proximity Forces // Ann. Phys. 1977. V. 105, Issue 2. P. 427–462.
11. *Dittrich B. et al.* Determination of Cross Sections for the Production of Be-7, Be-10 and Na-22 by High-Energy Protons // Radiochimica Acta. 1990. V. 50. P. 11.
12. *Michel R. et al.* Nuclide Production by Proton-Induced Reactions on Elements ($6 \leqslant Z \leqslant 29$) in the Energy Range from 800 to 2600 MeV // Nucl. Instrum. Meth. B. 1995. V. 103, Issue 2. P. 183–222.
13. *Titarenko Yu. E. et al.* Experimental and Theoretical Study of the Yields of Radioactive Product Nuclei in Tc-99 Thin Targets Irradiated with 100–2600 MeV Protons. USSR Report to the I.N.D.C. 2003. No. 434. P. 88.
14. Qtool: Calculation of Reaction Q-values and Thresholds. http://t2.lanl.gov/data/qtool.html
15. *Chu S. Y. F. et al.* The Lund/LBNL Nuclear Data Search Web Page. http://nucleardata.nuclear.lu.se/nucleardata/toi
16. *West J. T.* SABRINA: An Interactive Three-Dimensional Geometry-Modeling Program for MCNPX. LA-10688-M. 1986.
17. TALYS — Free Software for the Simulation of Nuclear Reactions. http://www.talys.eu
18. *Beckurts K. H., Wirtz K.* Neutron Physics. Berlin; Göttingen; Heidelberg; N. Y.: Springer-Verlag, 1964.
19. *Van Der Meer K. et al.* Spallation Yields of Neutrons Produced in Thick Lead/Bismuth Targets by Protons at Incident Energies of 420 and 590 MeV // Nucl. Instrum. Meth. Phys. Res. B. 2004. V. 217. P. 202–220.

Корректор *Т. Е. Попеко*